



# Fast long-axis strain: a simple, automatic approach for assessing left ventricular longitudinal function with cine cardiovascular magnetic resonance

Shuang Leng<sup>1</sup> · Ru-San Tan<sup>1,2</sup> · Xiaodan Zhao<sup>1</sup> · John C. Allen<sup>2</sup> · Angela S. Koh<sup>1,2</sup> · Liang Zhong<sup>1,2</sup> 

Received: 22 October 2019 / Revised: 7 February 2020 / Accepted: 12 February 2020 / Published online: 27 February 2020  
© European Society of Radiology 2020

## Abstract

**Objectives** In some cardiac pathologies, impairment of left ventricular (LV) longitudinal function may precede reduction in LV ejection fraction. This study investigates the effectiveness of a fast method to quantify long-axis LV function compared to conventional feature tracking and manual approaches.

**Methods** The study consisted of 50 normal controls and 100 heart failure (HF) patients including 40 with reduced ejection fraction (HFrEF), 30 with mid-range ejection fraction (HFmrEF), and 30 with preserved ejection fraction (HFpEF). Parameters including fast long-axis strain (FLAS) at end-systole and peak strain rates during systole (FLAS<sub>s</sub>), early diastole (FLAS<sub>e</sub>), and atrial contraction (FLAS<sub>a</sub>) were derived by a fast semi-automated approach on cine cardiovascular magnetic resonance.

**Results** FLAS exhibited good agreement with strain values obtained using conventional feature tracking (bias  $-2.9\%$ , limits of agreement  $\pm 3.0\%$ ) and the manual approach (bias  $0.6\%$ , limits of agreement  $\pm 2.1\%$ ), where FLAS was more reproducible and required shorter measurement time. The mean FLAS (HFrEF < HFmrEF < HFpEF < controls;  $6.1 \pm 2.4 < 9.9 \pm 2.4 < 11.0 \pm 2.5 < 16.9 \pm 2.3\%$ , all  $p < 0.0001$ ) was decreased in all the HF patient groups. A FLAS of  $12.3\%$  (mean-2SD of controls) predicted the presence of systolic dysfunction in  $67\%$  of patients with HFpEF, and  $87\%$  with HFmrEF. Strain parameters using the fast approach were superior to those obtained by conventional feature tracking and manual approaches for discriminating HFpEF from controls. Notable examples are area under the curve, sensitivity, and specificity for FLAS ( $0.94$ ,  $93\%$ , and  $86\%$ ) and FLAS<sub>e</sub> ( $0.96$ ,  $90\%$ , and  $94\%$ ).

**Conclusions** The fast approach-derived LV strain and strain rate parameters facilitate reproducible, reliable, and effective LV longitudinal function analysis.

## Key Points

- Left ventricular long-axis strain can be rapidly derived from cine CMR with shorter measurement time and higher reproducibility compared to conventional feature tracking and the manual approach.
- Progressive reductions in left ventricular long-axis strain and strain rate measurements were observed from HFpEF, HFmrEF, to HFrEF group.
- Based on long-axis strain, systolic abnormalities were evident in HFmrEF and HFpEF indicating common coexistence of systolic and diastolic dysfunction in the HF phenotypes.

**Keywords** Magnetic resonance imaging · Left ventricular function · Heart failure

**Electronic supplementary material** The online version of this article (<https://doi.org/10.1007/s00330-020-06744-6>) contains supplementary material, which is available to authorized users.

✉ Liang Zhong  
zhong.liang@nhcs.com.sg

<sup>1</sup> National Heart Research Institute Singapore, National Heart Centre Singapore, 5 Hospital Drive, Singapore 169609, Singapore

<sup>2</sup> Duke-NUS Medical School, National University of Singapore, 8 College Road, Singapore 169857, Singapore

## Abbreviations

ANOVA	Analysis of variance
AUC	Area under ROC curve
CMR	Cardiovascular magnetic resonance
CV	Coefficient of variation
DRA	Deformable registration-based analysis
EF	Ejection fraction
FLAS	Fast long-axis strain
FLASR	Fast long-axis strain rate

FT	Feature tracking
GTLS	Global transmural longitudinal strain
GTLSR	Global transmural longitudinal strain rate
HF	Heart failure
HFmrEF	Heart failure with mid-range ejection fraction
HFpEF	Heart failure with preserved ejection fraction
HFrfEF	Heart failure with reduced ejection fraction
LA	Left atrial
LV	Left ventricular
MAPSE	Mitral annular plane systolic excursion
MLAS	Manual long-axis strain
ROC	Receiver operating characteristic
SR	Strain rate
STE	Speckle tracking echocardiography

## Introduction

Systolic cardiac contraction is characterized by myocardial deformation in both longitudinal and circumferential directions. To date, left ventricular (LV) ejection fraction (EF) is most commonly used for assessing LV function and disease severity. However, one limitation of LVEF is its inability to entirely reflect the complexity of LV systolic function and distinguish functional impairment among different components of myocardial deformation. In some cardiac pathologies, impairment in longitudinal function may precede reductions in circumferential indices or global LVEF, leading to early LV pump dysfunction [1].

Assessment of myocardial deformation in the longitudinal direction, either by speckle tracking echocardiography (STE) [2] or cine cardiovascular magnetic resonance (CMR) feature tracking (FT-CMR) [3], may provide better insight into myocardial dysfunction with incremental value beyond LVEF. However, reproducibility of STE may be jeopardized by the use of differing analysis algorithms among various vendors [4]. Studies comparing four commercially available software packages for FT-CMR analysis have found that global and segmental myocardial strain values are not interchangeable between vendors [5, 6]. Hence, several prior studies have introduced a simple and vendor independent method for manually assessing long-axis strain based on differences of end-diastolic and end-systolic distances between LV apical epicardium and basal plane [7–10]. However, the approach yields only the LV end-systolic strain parameter and does not provide information about strain rate (SR) and diastolic function that in certain circumstances may better reflect cardiac function [11]. Herein, we aimed to (1) evaluate a fast semi-automated approach for assessing long-axis strain and SR for the dynamic determination of LV longitudinal function from standard cine CMR images and (2) perform comprehensive comparisons of strain measurements using the fast approach, conventional FT-CMR, and the manual approach. We hypothesized

that LV strain and SR derived using the fast approach would be non-inferior in terms of diagnostic accuracy, with shorter measurement time and increased reproducibility. In addition, an array of systolic and diastolic strain and SR parameters obtained using the fast approach can potentially contribute greater insight into progressive deterioration of myocardial contraction and relaxation in patients with heart failure (HF).

## Methods

### Study population

The study population consisted of 100 patients of which 40 had heart failure with reduced ejection fraction (HFrfEF, LVEF < 40%), 30 heart failure with mid-range ejection fraction (HFmrEF, LVEF 40–49%), and 30 heart failure with preserved ejection fraction (HFpEF, LVEF ≥ 50%). The LVEF range for each HF category was defined in [12]. Fifty age- and gender-matched normal controls were enrolled into the study. All subjects had normal sinus rhythm and no pacing artifact (existing device). The protocol was approved by the SingHealth Centralised Institutional Review Board and informed consent was obtained from all participants.

### CMR acquisition

Enrolled subjects underwent CMR scan using a 3 T magnetic resonance imaging system (Ingenia, Philips Healthcare). Steady-state free precession end-expiratory breath hold cine images were acquired in short- and long-axis views including the LV 2- and 4-chamber views. Typical CMR imaging parameters were as follows [13]: TR/TE, 3/1 ms; matrix, 240 × 240; flip angle, 45°; field of view, 300 × 300 mm<sup>2</sup>; pixel bandwidth, 1776 Hz; pixel spacing, 1.25 × 1.25 mm; slice thickness, 8 mm; number of cardiac frames, 30/40 per cardiac cycle.

In the present study, 41 subjects (25 normal controls and 16 HFrfEF patients) had undergone CMR tagging studies. Grid tag spacing was 7 mm. Other typical scan parameters can be found in the [Supplemental material](#).

### Global transmural longitudinal strain by feature tracking

Dedicated QStrain software (version 2.0, Medis) was used in deriving LV longitudinal strain. End-systole was identified visually from the cine images. Endocardial and epicardial contours were manually delineated in the end-diastolic and end-systolic frames. Automatic contour tracking was then performed by tracking 48 evenly spaced points along the contour [3]. In case of insufficient tracking, contours were manually corrected and the algorithm reapplied. Global transmural

longitudinal strain (GTLS) representing the mean value of endocardial and epicardial strains at end-systole was measured [7]. Average GTLS values in 2- and 4-chamber views were calculated for analysis (Fig. 1 right column). SR results (denoted by global transmural longitudinal strain rate (GTLSR)) were obtained by taking the first-order derivative of the strain curve.

### Manual long-axis strain

Manual LV strain assessment was performed as described previously [7, 8]. In brief, the mitral valve insertion points and the epicardial apex were manually located in both end-systole and end-diastole. This was then followed by measuring the distance between the epicardial apex and the middle of

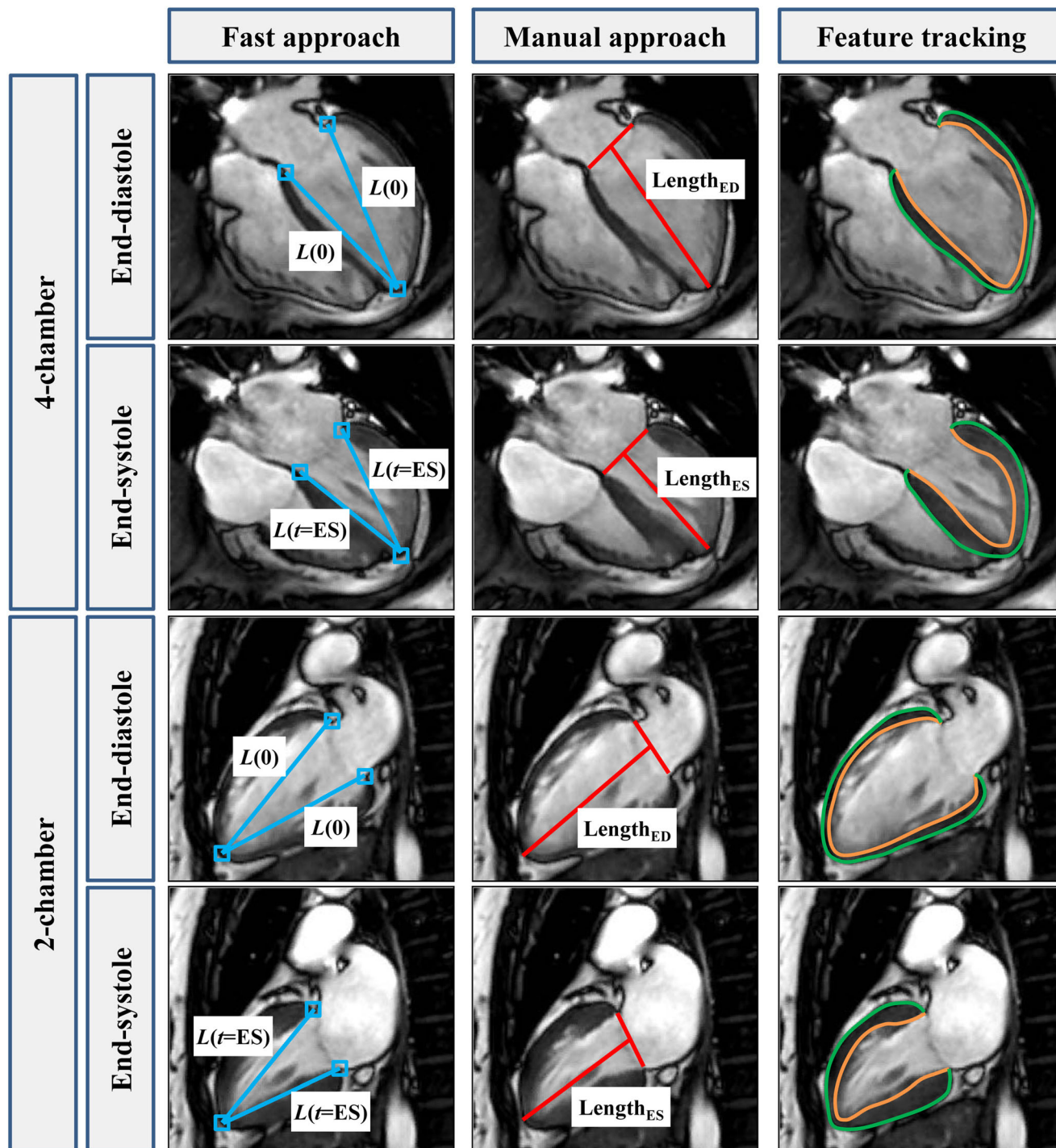


**Fig. 1** Left ventricular long-axis strain measurement in 4- and 2-chamber views using left column, fast approach; middle column, manual approach; right column, feature tracking approach. *ED* end-diastole, *ES* end-systole. For details, see text

a line connecting the mitral valve insertions. The difference in end-diastolic and end-systolic distances was normalized to the end-diastolic distance for the calculation of manual long-axis strain (MLAS) which represents the strain value at end-systole:  $MLAS = (\text{Length}_{\text{end-systole}} - \text{Length}_{\text{end-diastole}}) \times 100 / \text{Length}_{\text{end-diastole}}$ . Final MLAS values were based on the average of 2- and 4-chamber views (Fig. 1 middle column).

### Fast long-axis strain

The strain assessment with the fast approach was performed by automatically tracking the distance ( $L$ ) from the mitral valve insertions to the epicardial apex on CMR 2- and 4-chamber views (Fig. 1 left column). The tracking system was developed using MATLAB (version R2018b, MathWorks Inc.) and consisted of the following steps [14]:

- Step 1 (manual): A small square (called mask) was manually drawn in the LV end-diastolic frame containing the anatomical point of interest (squares in Fig. 1 left column). Typical mask size of  $8 \times 8$  pixels was used.
- Step 2 (automatic): A search region sharing the same center with the selected mask was automatically generated in the target frame (i.e., the next temporal frame). The size of the search region was  $20 \times 20$  pixels.
- Step 3 (automatic): Template matching algorithm [15] was conducted to detect the best match of the mask in the target frame, within the search region based on normalized cross correlation criterion.
- Step 4 (automatic): The location of the best match was used to update the mask in the target frame and the same procedure (Steps 2–4) was automatically executed iteratively for all subsequent frames throughout the cardiac cycle.

Longitudinal strain at any time point ( $t$ ) in the cardiac cycle from LV end-diastole (time 0) was calculated as  $(L(t) - L(0)) \times 100 / L(0)$ . Fast long-axis strain (FLAS) was defined as the strain value at LV end-systole (i.e.,  $t = \text{LV end-systole}$ ), and the strain rates FLASR were derived as peak values during systole (FLASR<sub>s</sub>), early diastole (FLASR<sub>e</sub>), and atrial contraction (FLASR<sub>a</sub>), respectively (Fig. 2). Fast strain and SR parameters from both 2- and 4-chamber views were averaged to obtain mean results for analysis. As LV strain and systolic SR are negative, we took their absolute values for a simple interpretation.

### CMR assessment of mitral annular dynamics

The following mitral annular dynamic measurements were calculated based on the tracking of mitral valve insertion points: (1) peak velocities during systole ( $S'$ ), early diastole ( $E'$ ), and atrial contraction ( $A'$ ) and (2)

mitral annular plane systolic excursion (MAPSE). Descriptions of the CMR-derived  $S'$ ,  $E'$ ,  $A'$ , and MAPSE measurements were detailed in prior studies [16–18].

### Intra- and inter-observer reproducibility and time requirements

Intra- and inter-observer variability were studied on a randomly selected subgroup of 20 cases (10 normal controls and 10 patients) using Bland-Altman analysis and coefficient of variation (CV). The time required for the measurement of FLAS, MLAS, and GTLS, which included the time for all the non-automatic steps, were recorded in the selected 20 cases.

### Statistical analysis

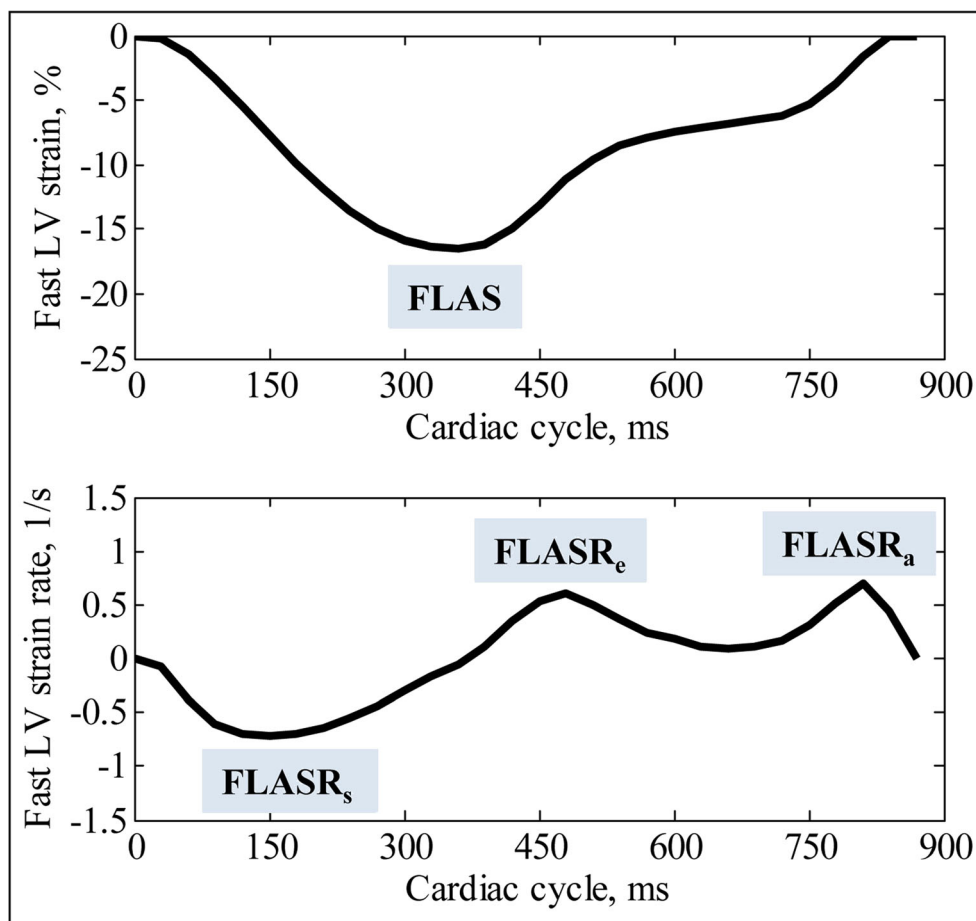
Statistical analysis was conducted using SPSS (version 17.0, IBM). Continuous data were summarized as mean  $\pm$  SD. For the comparisons of characteristics and strain data between patient groups and control subjects, the one-way analysis of variance (ANOVA)  $F$ -test was used first to test the overall difference among the means of all subject groups. If an overall statistically significant difference in group means (i.e., a statistically significant one-way ANOVA  $F$ -test with  $p$  value  $< 0.05$ ) was demonstrated, it was followed up with post hoc tests for pairwise multiple comparisons. Tukey's honestly significant difference post hoc test was used when the data met the assumption of variance homogeneity, and Games Howell post hoc test was used if the data did not meet the assumption. Pearson's  $r$  correlation, Passing-Bablok non-parametric regression, and Bland-Altman plots were used to assess the agreement of FLAS data with respect to GTLS and MLAS. The association between FLAS and LVEF was assessed using the coefficient of determination ( $R^2$ ) as the goodness-of-fit measure. Receiver operating characteristic (ROC) analysis was conducted to determine the capability of strain measurements for discriminating patients from normal controls. Youden's index was defined for all points of an ROC curve, and the maximum value of the index was used as the criterion for selecting the optimum threshold point. A  $p$  value less than 0.05 was considered statistically significant.

### Results

Baseline demographics and clinical characteristics of controls and HF patients are presented in Table 1. There were no significant differences among the groups in age, gender, and body surface area.



**Fig. 2** Left ventricular strain and strain rate variables. Fast long-axis strain (FLAS): defined as the strain value at LV end-systole; peak systolic fast long-axis strain rate (FLASR<sub>s</sub>): defined as the peak strain rate value during systole; peak early diastolic fast long-axis strain rate (FLASR<sub>e</sub>): defined as the peak strain rate value during early diastole; peak late diastolic fast long-axis strain rate (FLASR<sub>a</sub>): defined as the peak strain rate value during late diastole (i.e., atrial contraction)



### Validation of fast approach–derived strain data

Figure 3 shows the median  $\pm$  interquartile range of time normalized strain and SR curves derived by the fast approach in the subjects from control, HFpEF, HFmrEF, and HFrfEF group, respectively. In all subjects, FLAS showed an excellent correlation with MLAS ( $r = 0.98$ ,  $p < 0.0001$ ) and GTLS ( $r = 0.96$ ,  $p < 0.0001$ ). Bland-Altman plots revealed a bias of 0.6% between FLAS and MLAS with limits of agreement of  $\pm 2.1\%$ ; bias between FLAS and GTLS was  $-2.9\%$  with limits of agreement of  $\pm 3.0\%$  (Supplementary Fig. 1). Fast SR measurements exhibited strong correlation with FT-based SRs ( $r = 0.94$  between FLASR<sub>s</sub> and GTLSR<sub>s</sub>; 0.87 between FLASR<sub>e</sub> and GTLSR<sub>e</sub>; and 0.87 between FLASR<sub>a</sub> and GTLSR<sub>a</sub>, all  $p < 0.0001$ ) (Supplementary Fig. 2).

Comparison with tagging has also been performed as an addition to the validation. Tagged image analysis procedure using CIM software [19] (CIMTag2D version 8.1.6, Auckland MRI Research Group) in 2- and 4-chamber views can be found in the [Supplemental material](#) and Supplementary Fig. 3. Global longitudinal strain value at end-systole (GLS<sub>tag</sub>) was recorded. In those subjects who have undergone tagging studies ( $n = 41$ ), excellent correlation was observed between FLAS and GLS<sub>tag</sub> ( $r = 0.98$ ,  $p < 0.0001$ ) with a bias of  $-0.2\%$  and limits of agreement

of  $\pm 1.3\%$  (Supplementary Fig. 4). Our fast strain assessment approach automatically tracked the discrete reference points throughout the cardiac cycle. Assessment of the tracking accuracy by comparison with manual selection of the reference points (mitral insertions and apex) was performed in parallel in a subset of the cohort ( $n = 40$ , 10 controls, 10 HFpEF, 10 HFmrEF, 10 HFrfEF). Results showed that the fast approach–derived strain and SR measurements were in good agreement with the manually derived results (Supplementary Table 1).

### Systolic parameters

Progressive reductions in S' velocity and MAPSE from HFpEF, HFmrEF, to HFrfEF group were observed (Table 1). FLAS and FLASR<sub>s</sub> in HF patients were significantly lower than in control subjects. It was found that ordering FLAS from largest to smallest in the patient group gave HFpEF > HFmrEF > HFrfEF ( $11.0 \pm 2.5 > 9.9 \pm 2.4 > 6.1 \pm 2.4\%$ ), where the difference was significant between any two groups ( $p < 0.0001$ ) (Table 2). In assessing the relationship between FLAS and LVEF, a scatter plot was generated using the combined data from the entire subject cohort (Fig. 4). It is readily observed from the scatter plot that the relationship between LVEF and FLAS is curvilinear; hence, a quadratic function was used to fit the data and the fitted regression equation was LVEF =

**Table 1** Baseline demographic and clinical characteristics of study subjects

Variables	Controls (n = 50)	HFpEF (n = 30)	HFmrEF (n = 30)	HFrEF (n = 40)	Overall p value
Age, years	56 ± 13	62 ± 11	57 ± 10	56 ± 10	0.209
Gender, male/female	34/16	23/7	20/10	29/11	0.804
BSA, m <sup>2</sup>	1.7 ± 0.2	1.8 ± 0.2	1.9 ± 0.2	1.8 ± 0.3	0.080
DBP, mmHg	78 ± 10	81 ± 24	76 ± 12	73 ± 14	0.249
SBP, mmHg	135 ± 18	142 ± 26	134 ± 22	122 ± 19*#	0.002
NYHA class	1.0 ± 0.0	1.6 ± 0.5*	1.8 ± 0.7*	2.1 ± 0.9*#	< 0.0001
NT-pro-BNP, pg/ml <sup>a</sup>	–	229 (113, 608)	479 (304, 781)#	2079 (807, 4930)#\$	< 0.0001
Medications (%)					
Diuretics	0 (0%)	21 (70%)*	23 (77%)*	39 (98%)*	< 0.0001
ACE inhibitor/angiotensin receptor blocker	0 (0%)	24 (80%)*	22 (73%)*	29 (73%)*	< 0.0001
β-Blocker	0 (0%)	23 (77%)*	20 (67%)*	36 (90%)*	< 0.0001
Aspirin	0 (0%)	17 (57%)*	15 (50%)*	20 (50%)*	< 0.0001
LV EDV index, ml/m <sup>2</sup>	70 ± 11	78 ± 16	87 ± 19*	138 ± 35*#	< 0.0001
LV ESV index, ml/m <sup>2</sup>	26 ± 6	34 ± 8*	50 ± 11*#	105 ± 35*#	< 0.0001
LV SV index, ml/m <sup>2</sup>	45 ± 8	44 ± 9	38 ± 9	33 ± 11*#	< 0.0001
LV EF, %	64 ± 6	56 ± 4*	44 ± 3*#	26 ± 8*#	< 0.0001
LV mass index, g/m <sup>2</sup>	48 ± 10	85 ± 39*	63 ± 19*	82 ± 21*	< 0.0001
S', cm/s	8.1 ± 1.4	6.3 ± 1.0*	5.4 ± 1.3*#	4.1 ± 0.9*#	< 0.0001
E', cm/s	9.5 ± 2.5	5.2 ± 1.4*	5.3 ± 1.5*	4.2 ± 1.1*#	< 0.0001
A', cm/s	8.8 ± 1.8	7.1 ± 1.7*	5.5 ± 1.9*#	3.7 ± 1.7*#	< 0.0001
MAPSE, mm	15.4 ± 1.8	12.0 ± 1.7*	10.6 ± 2.6*#	7.9 ± 2.6*#	< 0.0001

Data are represented as mean ± SD, median (interquartile range), or n (%)

BSA body surface area; DBP diastolic blood pressure; SBP systolic blood pressure; NYHA New York Heart Association; NT-pro-BNP N-terminal pro-brain natriuretic peptide; LV left ventricular; EDV end-diastolic volume; ESV end-systolic volume; SV stroke volume; EF ejection fraction; S', E', A' peak systolic, early diastolic, and late diastolic mitral annular velocities; MAPSE mitral annular plane systolic excursion; HFpEF heart failure with preserved ejection fraction; HFmrEF heart failure with mid-range ejection fraction; HFrEF heart failure with reduced ejection fraction

\*Significant difference compared to controls; #significant difference compared to HFpEF; \$significant difference compared to HFmrEF

<sup>a</sup> NT-pro-BNP were not available for controls; NT-pro-BNP were available in 20 HFpEF, 20 HFmrEF, and all HFrEF patients

0.1201 + 5.9996 FLAS – 0.1343 FLAS<sup>2</sup> with R<sup>2</sup> = 0.75. To compare FLAS with LVEF, the value of – 2 SD from the mean FLAS in the control subjects (i.e., 12.3%) was used as the cutoff point for abnormality. It was found that 67% of patients with HFpEF had FLAS < 12.3% and was 87% in the HFmrEF group.

**Diastolic parameters**

Significantly reduced E', A', FLASR<sub>e</sub>, and FLASR<sub>a</sub> were observed in all patient groups when compared with control subjects (Tables 1 and 2). FLASR<sub>e</sub> and FLASR<sub>a</sub> were lower in patients with HFrEF than in those with HFmrEF and HFpEF, while these parameters were not significantly different between HFmrEF and HFpEF (Table 2).

**Detection of HFpEF**

Compared to standard clinical parameters and strain measurements obtained using the manual approach and conventional FT, fast LV strain achieved higher levels of accuracy and greater areas under ROC curves (AUCs) in differentiating HFpEF from normal controls (Table 3 and Fig. 5). The best variables for detecting HFpEF were FLAS (AUC = 0.94, sensitivity = 93%, and specificity = 86%) and FLASR<sub>e</sub> (AUC = 0.96, sensitivity = 90%, and specificity = 94%).

**Reproducibility and time requirement**

Intra- and inter-observer CVs for FLAS were 2.9% and 3.4% (Table 4). Intra-observer CVs were 5.8% for GTLS and 5.4% for MLAS, with corresponding inter-observer CVs of 7.0% and 6.4%, respectively. FLASR measurements were more reproducible than GTLSR as reflected by narrower limits of agreement and lower CVs (Table 4). The mean ± SD time per subject required for fast LV strain measurement was 78 ± 8 s, which was shorter than the mean measurement time of 90 ± 7 s using manual approach and 180 ± 12 s using FT approach.

**Discussion**

The current study demonstrated the feasibility and effectiveness of a fast semi-automated long-axis strain method for assessing longitudinal LV function using CMR cine images. Comprehensive comparisons among different methods exhibited good agreement between FLAS and strains measured using either the conventional FT-CMR or the manual approaches. FLAS performed better at differentiating HFpEF from normal controls than did MLAS and GTLS, as well as other LV parameters such as LVEF and MAPSE. Finally, measurement time for FLAS was shorter with higher reproducibility compared to those for MLAS and GTLS.

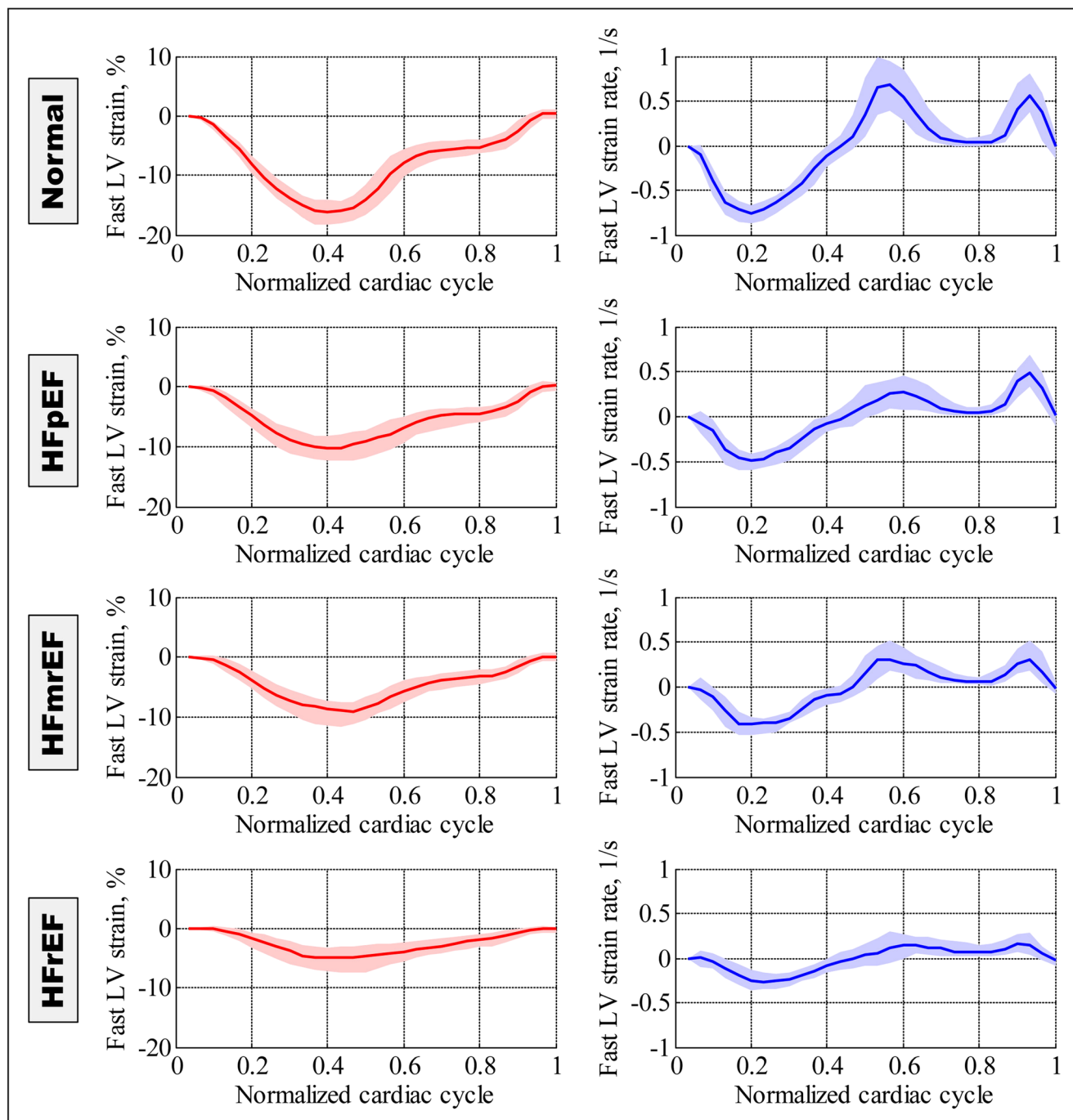


**Fig. 3** Median (solid line)  $\pm$  interquartile range (shaded area) of time normalized strain and strain rate curves derived by the fast approach in all subjects from control, HFpEF, HFmrEF, and HFrEF group, respectively

### Clinical aspect: LV longitudinal function in HFpEF, HFmrEF, and HFrEF

We performed fast LV strain measurements in the three HF phenotypes and found progressive reductions in FLAS and FLASR from HFpEF, HFmrEF, to HFrEF group.

Peak early diastolic SR has been used in prior studies as an independent parameter, or in combination with early mitral inflow velocity, for the assessment of diastolic abnormalities

in various patient groups [20, 21]. Studies have demonstrated that patients with HFpEF exhibited significantly reduced early diastolic longitudinal SR when compared to asymptomatic patients [22] and controls subjects [23]. Our study corroborated previous findings that FLASR<sub>e</sub> and FLASR<sub>a</sub> were significantly decreased in HFpEF patients in comparison to age- and gender-matched normal controls. In addition, ROC analysis demonstrated non-inferior (slightly better) diagnostic performance for FLASR<sub>e</sub> over GTLSR<sub>e</sub> and conventional LV

**Table 2** Comparisons of fast left ventricular strain and strain rate measurements among subject groups

Variables	Controls (n = 50)	HFpEF (n = 30)	HFmrEF (n = 30)	HFrEF (n = 40)	Overall p value
FLAS, %	16.9 ± 2.3	11.0 ± 2.5*	9.9 ± 2.4*#	6.1 ± 2.4*##\$	< 0.0001
FLAS <sub>s</sub> , 1/s	0.9 ± 0.1	0.6 ± 0.2*	0.6 ± 0.2*	0.3 ± 0.1*##\$	< 0.0001
FLAS <sub>e</sub> , 1/s	1.1 ± 0.2	0.5 ± 0.2*	0.5 ± 0.1*	0.4 ± 0.1*##\$	< 0.0001
FLAS <sub>a</sub> , 1/s	0.8 ± 0.2	0.7 ± 0.2*	0.5 ± 0.2*	0.3 ± 0.1*##\$	< 0.0001

Data are represented as mean ± SD

FLAS fast long-axis strain; FLAS<sub>s</sub> peak systolic fast long-axis strain rate; FLAS<sub>e</sub> peak early diastolic fast long-axis strain rate; FLAS<sub>a</sub> peak fast long-axis strain rate during atrial contraction; HFpEF heart failure with preserved ejection fraction; HFmrEF heart failure with mid-range ejection fraction; HFrEF heart failure with reduced ejection fraction

\*Significant difference compared to controls; #significant difference compared to HFpEF; \$significant difference compared to HFmrEF

diastolic function measurements (e.g., E') in differentiating HFpEF patients from controls.

Previous evaluations of LV systolic function in HFpEF have yielded contradictory results. For example, a previous study using STE found that global longitudinal strain was preserved in patients with HFpEF compared to age-matched older controls [24], while other tissue Doppler studies showed abnormalities in systolic mitral annular motion in HFpEF [25]. In the present study, FLAS and FLAS<sub>s</sub> were found to be significantly lower in HFpEF compared to normal controls, indicating that systolic function was indeed impaired in these patients. FLAS was significantly correlated with measures of diastolic function (FLAS vs. FLAS<sub>e</sub>,  $r = 0.83$ ; FLAS vs. E',  $r = 0.54$ ; both  $p < 0.0001$ ), which was in line with prior findings that the systolic abnormalities probably coexist with diastolic dysfunction in HFpEF—a condition not reflected by conventional measures such as LVEF [26]. The underlying

pathophysiology is that the functional abnormalities of intracellular calcium handling and myofilament interaction resulting in diastolic abnormalities may also affect systolic function [27]. In addition, HFpEF patients have higher LV mass (hypertrophy) compared to healthy controls, which was confirmed in the current study. Over time, the increasing LV systolic and diastolic stiffness leads to progressive deterioration of LV longitudinal contraction and relaxation [28]. Our study demonstrated an inverse correlation between FLAS and LV mass index in HFpEF ( $r = -0.57$ ,  $p < 0.0001$ ), revealing adverse association between LV hypertrophy and LV systolic function.

While it is well accepted that HFmrEF is a distinct clinical group situated between HFpEF and HFrEF with intermediate clinical, structural, and functional characteristics, uncertainties remain with respect to HFmrEF. It has been reported that HFmrEF patients conformed a phenotype closer to the

**Fig. 4** Scatterplot for FLAS and LVEF in patients with HFpEF, HFmrEF, and HFrEF and in normal control subjects. Note difference in distribution of points with respect to ejection fraction of 50% and FLAS of 12.3% (2 SD below mean of control subjects). A quadratic regression model was used to fit the data

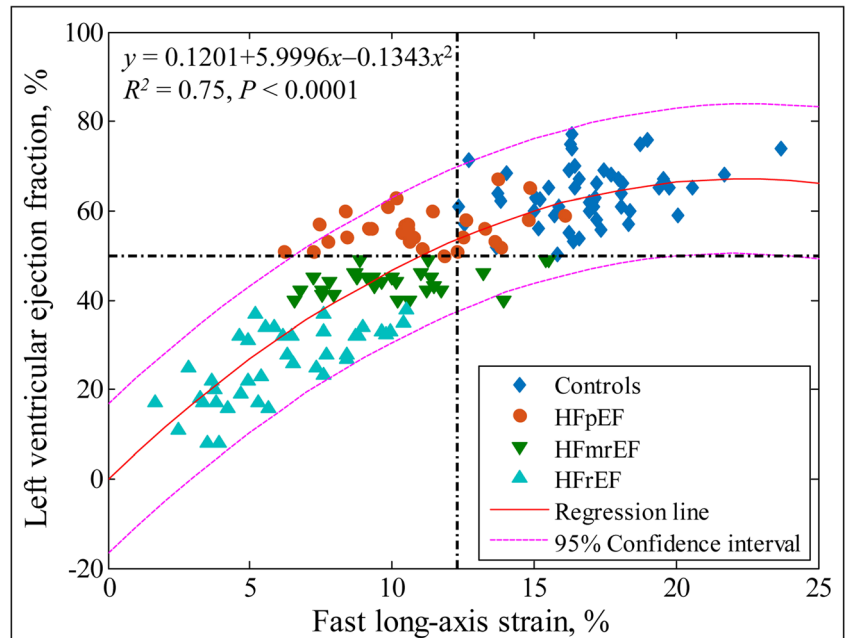




**Table 3** Utility of left ventricular strain and strain rate measurements using fast, conventional feature tracking, and manual approaches, as well as standard clinical parameters to differentiate patients with HFpEF from controls: results of the receiver operating characteristic (ROC) analysis with area under the curve (AUC), sensitivity, specificity, and threshold

Variables	AUC (95% CI)	Sensitivity (95% CI)	Specificity (95% CI)	Threshold
<b>Systolic parameters</b>				
FLAS, %	0.94 (0.86, 0.98)	93 (78, 99)	86 (73, 94)	14.9
MLAS, %	0.89 (0.80, 0.95)	83 (65, 94)	88 (76, 96)	13.4
GTLS, %	0.86 (0.77, 0.93)	77 (58, 90)	92 (81, 98)	16.7
FLASR <sub>s</sub> , 1/s	0.82 (0.72, 0.90)	70 (51, 85)	94 (84, 99)	0.66
GTLSR <sub>s</sub> , 1/s	0.78 (0.67, 0.86)	73 (54, 88)	86 (73, 94)	0.81
S', cm/s	0.87 (0.77, 0.93)	93 (78, 99)	76 (62, 87)	7.2
MAPSE, mm	0.92 (0.84, 0.97)	87 (69, 96)	90 (78, 97)	13.2
LVEF, %	0.82 (0.72, 0.90)	80 (61, 92)	76 (62, 87)	60.0
<b>Diastolic parameters</b>				
FLASR <sub>e</sub> , 1/s	0.96 (0.89, 0.99)	90 (74, 98)	94 (84, 99)	0.77
FLASR <sub>a</sub> , 1/s	0.73 (0.62, 0.82)	77 (58, 90)	60 (45, 74)	0.76
GTLSR <sub>e</sub> , 1/s	0.89 (0.80, 0.95)	80 (61, 92)	84 (71, 93)	0.78
GTLSR <sub>a</sub> , 1/s	0.62 (0.50, 0.72)	60 (41, 77)	64 (49, 77)	0.76
E', cm/s	0.95 (0.89, 0.99)	87 (69, 96)	94 (84, 99)	6.3
A', cm/s	0.77 (0.66, 0.86)	63 (44, 80)	84 (71, 93)	7.3

CI confidence interval; FLAS fast long-axis strain; MLAS manual long-axis strain; GTLS global transmural longitudinal strain; FLASR, peak systolic fast long-axis strain rate; GTLSR<sub>s</sub> peak systolic global transmural longitudinal strain rate; S' peak systolic mitral annular velocity; MAPSE mitral annular plane systolic excursion; LVEF left ventricular ejection fraction; FLASR<sub>e</sub> peak early diastolic fast long-axis strain rate; FLASR<sub>a</sub> peak fast long-axis strain rate during atrial contraction; GTLSR<sub>e</sub> peak early diastolic global transmural longitudinal strain rate; GTLSR<sub>a</sub> peak global transmural longitudinal strain rate during atrial contraction; E' peak early diastolic mitral annular velocity; A' peak mitral annular velocity during atrial contraction

**Fig. 5** Detection of HFpEF: ROC curves comparing the diagnostic performance of FLASR<sub>e</sub>, FLAS, MLAS, GTLS, and LVEF with respective AUC values. The optimal cutoff value for each parameter is demonstrated with a circle. FLASR<sub>e</sub> peak early diastolic fast long-axis strain rate, FLAS fast long-axis strain, MLAS manual long-axis strain, GTLS global transmural longitudinal strain, LVEF left ventricular ejection fraction

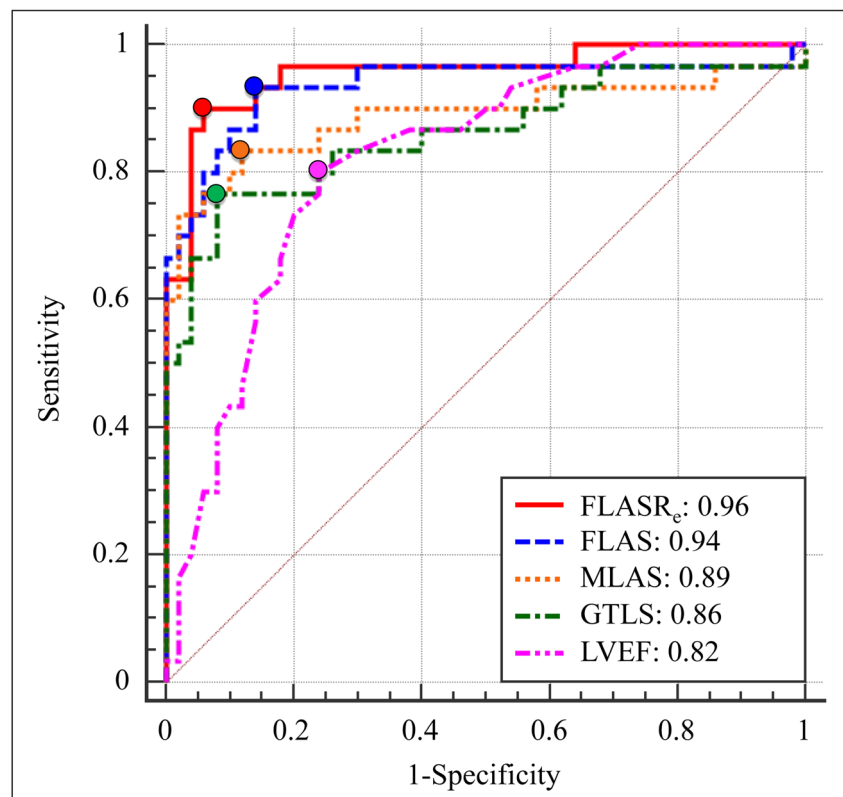


**Table 4** Intra- and inter-observer reproducibility for left ventricular strain and strain rate measurements derived by fast, conventional feature tracking, and manual approaches

Method	Strain/strain rate	Intra-observer ( <i>n</i> = 20)		Inter-observer ( <i>n</i> = 20)	
		Bias (limits of agreement)	CV, %	Bias (limits of agreement)	CV, %
Fast approach	FLAS, %	0.1 (− 1.0, 1.2)	2.9	0.3 (− 1.0, 1.5)	3.4
	FLAS <sub>s</sub> , 1/s	0.002 (− 0.092, 0.096)	4.7	0.021 (− 0.064, 0.105)	4.7
	FLAS <sub>e</sub> , 1/s	0.022 (− 0.081, 0.125)	4.8	0.032 (− 0.132, 0.195)	7.5
	FLAS <sub>a</sub> , 1/s	− 0.005 (− 0.073, 0.062)	3.6	0.003 (− 0.099, 0.104)	5.3
Feature tracking approach	GTLS, %	− 0.2 (− 3.1, 2.8)	5.8	− 0.8 (− 3.9, 2.4)	7.0
	GTLS <sub>s</sub> , 1/s	− 0.023 (− 0.221, 0.176)	8.2	− 0.010 (− 0.232, 0.213)	8.9
	GTLS <sub>e</sub> , 1/s	0.022 (− 0.142, 0.187)	6.3	− 0.007 (− 0.188, 0.174)	6.8
	GTLS <sub>a</sub> , 1/s	− 0.021 (− 0.229, 0.188)	10.5	− 0.011 (− 0.238, 0.217)	11.2
Manual approach	MLAS, %	− 0.1 (− 1.9, 1.8)	5.4	− 0.5 (− 2.6, 1.7)	6.4

FLAS fast long-axis strain; FLAS<sub>s</sub> peak systolic fast long-axis strain rate; FLAS<sub>e</sub> peak early diastolic fast long-axis strain rate; FLAS<sub>a</sub> peak fast long-axis strain rate during atrial contraction; GTLS global transmural longitudinal strain; GTLS<sub>s</sub> peak systolic global transmural longitudinal strain rate; GTLS<sub>e</sub> peak early diastolic global transmural longitudinal strain rate; GTLS<sub>a</sub> peak global transmural longitudinal strain rate during atrial contraction; MLAS manual long-axis strain; CV coefficient of variation

HFmrEF clinical profile [29]. However, other registries showed that HFmrEF patient prognosis was similar to that of HFpEF [30]. Findings in the current study suggested that in HFmrEF patients, FLAS was significantly impaired while FLAS<sub>e</sub> was comparable to HFpEF patients. Given the fact that FLAS is a more sensitive and accurate metric for LV longitudinal function, it could become invaluable as a CMR parameter to assess severity with the potential to refine HFmrEF patient risk stratification. It is plausible that clinical monitoring of either FLAS or FLAS<sub>e</sub> over time in HFmrEF patients may provide important predictive insights into their clinical trajectories toward either HFpEF or HFmrEF.

The left atrial (LA) function of the same subject cohort had been assessed in a prior study [13]. A significant correlation between FLAS and LA global reservoir strain  $\epsilon_s$  was observed ( $r = 0.87$ ,  $p < 0.0001$ ), suggesting that as LV longitudinal function worsens, so does the LA reservoir function [31]. Indeed, the degree of LV longitudinal contraction and the LA myocardial compliance are the two major determinants of LA relaxation [32]. The presented techniques facilitate understanding of LV-LA kinematic interaction, which will potentially be useful for investigating the association with clinical status of the patients and disease progression.

**Technical aspect: Fast vs. feature tracking vs. manual long-axis strain**

Prior studies have utilized GTLS by FT-CMR for characterization of myocardial function in both adult and pediatric populations [33, 34]. GTLS can be calculated by using the entire myocardial line length while computing the deformation. Alternatively, GTLS can also be derived by averaging the values computed in each individual point within the myocardial line

(used in the current study with 48 points along the contour), or by averaging the values computed at the segmental level from the same frame [35]. It is worth noting that calculation of GTLS, either by using the entire myocardial length or by averaging values computed at point or segmental level, will give different results [35–37]. Furthermore, the routine clinical implementation of FT-CMR is limited by undisclosed technical properties in existing software and numerical differences in some strain parameters among software versions [8].

Instead of an analysis that encompasses the entire LV myocardium, multiple prior studies have introduced simple and vendor independent methods for manually assessing long-axis strain based on differences of end-diastolic and end-systolic distances between the LV apical epicardium and the basal plane [7–10]. Riffel et al [7] assessed the longitudinal function of the LV with CMR using the long-axis strain manually derived from the distance of the epicardial apical border to the mid-point of the line connecting the mitral valve insertion points (LAS-epi/mid). The LAS-epi/mid demonstrated high correlation with conventional FT analysis results, and was non-inferior in discriminating patients with cardiomyopathies from healthy controls. The prognostic importance of LAS-epi/mid was explored in the study by Schuster et al [8] in patients with acute myocardial infarction, where LAS-epi/mid remained significantly associated with higher occurrence of major adverse clinical events after correction for established risk stratification parameters. This technique is not limited to CMR and has also been applied to echocardiography. In a group of patients with dilated cardiomyopathy, Aurich et al [10] introduced an echocardiographic unidimensional long-axis strain metric with diagnostic properties comparable to STE-based global longitudinal strain and superior to other conventional longitudinal function parameters.

The manual approach-derived MLAS provides an easy approximation of longitudinal deformation. However, unlike FT-CMR, the manual approach yields only the LV end-systolic strain parameter and does not provide information on SR and diastolic function that may better reflect cardiac function under certain circumstances. Our fast approach took one step forward in applying semi-automatic tracking of only 3 anatomically discrete points, drawing on respective advantages of manual and conventional FT-based methods and allowing for dynamic evaluation of LV longitudinal function. Most importantly, current study demonstrated that the fast approach offered high reliability and comparability to conventional approaches, and required shorter time for strain measurement. Investigation into the reproducibility of the technique in repeat acquisitions, not just repeat analyses, warrants further study, as this would increase confidence in true reproducibility. Deformable registration-based analysis (DRA) tool—an alternative method to FT-CMR—has been used for analyzing myocardial strain from the cine images [38]. Future studies are needed regarding the comparison between the fast and the DRA approaches.

## Limitations

The fast LV strain is an index of global LV function in the longitudinal direction, and unable to provide information on circumferential and radial strains. Although FLAS and GTLS are both measures of longitudinal LV deformation, lower values for FLAS were found in the Bland-Altman plot (bias  $-2.9\%$ ). This systematic underestimation may be due to a geometric factor [10]. While FT method tracks the entire deformation contour during the cardiac cycle, the fast approach tracks the lines connecting mitral valve insertions and the epicardial apex. The epicardial apex remains relatively stationary, and the mitral valve insertions demonstrate arc-like motions not only toward the apex but also to the side during systole. Therefore, the line deformation will always be lower in this case compared to the case when motion is restricted only to the direction toward the apex with the same distance traveled by the mitral valve insertions [10]. In the equation used for FLAS derivation, “ $L$ ” was defined as the distance from the mitral valve insertions to the epicardial apex. This was different from the distance used for MLAS calculation, which is the distance from the mid-point of the line joining the mitral valve insertions to the apex. This may be the cause of the small systematic differences in strains measured with the two techniques. SR measurements were not derived using the manual approach as it is not clinically practical to manually measure distance in every CMR frame over the cardiac cycle.

## Conclusions

The fast LV strain measurements represent robust and easily calculated parameters for quantifying long-axis LV

deformation using routine cine CMR images in the clinical setting. Fast LV strain measurements exhibited high correlation with those obtained using manual and conventional FT approaches, were superior for discriminating patients with HFpEF from normal controls, were more reproducible, and required shorter measurement time.

**Funding information** This study received funding support from the National Medical Research Council Singapore (NMRC/OFIG/0018/2016; NMRC/BnB/0017/2015; MOH-000358; MOH-000351; NMRC/TA/0031/2015; MOH-000153), SingHealth Duke-NUS Academic Medicine Research Grant (AM/TP015/2018 (SRDUKAMR1814)). The funder had no role in the design and conduct of the study; collection; management, analysis, and interpretation of the data; and preparation, review, or approval of the manuscript.

## Compliance with ethical standards

**Guarantor** The scientific guarantor of this publication is Liang Zhong.

**Conflict of interest** The authors of this manuscript declare no relationships with any companies whose products or services may be related to the subject matter of the article.

**Statistics and biometry** One of the authors has significant statistical expertise (John C. Allen, statistician, Duke-NUS Medical School, Singapore).

**Informed consent** Written informed consent was obtained from all subjects (patients) in this study.

**Ethical approval** Institutional Review Board approval was obtained.

**Study subjects or cohorts overlap** Study subjects or cohorts have been reported in a previously published paper (Leng S et al Validation of a rapid semi-automated method to assess left atrial longitudinal phasic strains on cine cardiovascular magnetic resonance imaging. *J Cardiovasc Magn Reson* 2018;20:71). However, the prior report focused on the left atrial function assessment. The current study investigated the left ventricular function assessed by a fast method compared to conventional feature tracking and manual approaches.

## Methodology

- Prospective
- Diagnostic or prognostic study
- Performed at one institution

## References

1. Kraigher-Krainer E, Shah AM, Gupta DK et al (2014) Impaired systolic function by strain imaging in heart failure with preserved ejection fraction. *J Am Coll Cardiol* 63:447–456
2. Abraham TP, Dimaano VL, Liang HY (2007) Role of tissue Doppler and strain echocardiography in current clinical practice. *Circulation* 116:2597–2609
3. Schuster A, Hor KN, Kowallick JT, Beerbaum P, Kutty S (2016) Cardiovascular magnetic resonance myocardial feature tracking: concepts and clinical applications. *Circ Cardiovasc Imaging* 9:e004077

4. Cikes M, Solomon SD (2016) Beyond ejection fraction: an integrative approach for assessment of cardiac structure and function in heart failure. *Eur Heart J* 37:1642–1650
5. Barreiro-Pérez M, Curione D, Symons R, Claus P, Voigt JU, Bogaert J (2018) Left ventricular global myocardial strain assessment comparing the reproducibility of four commercially available CMR-feature tracking algorithms. *Eur Radiol* 28:5137–5147
6. Dobrovic M, Barreiro-Pérez M, Curione D et al (2019) Inter-vendor reproducibility and accuracy of segmental left ventricular strain measurements using CMR feature tracking. *Eur Radiol* 29:6846–6857
7. Riffel JH, Andre F, Maertens M et al (2015) Fast assessment of long axis strain with standard cardiovascular magnetic resonance: a validation study of a novel parameter with reference values. *J Cardiovasc Magn Reson* 17:69
8. Schuster A, Backhaus SJ, Stiermaier T et al (2019) Fast manual long-axis strain assessment provides optimized cardiovascular event prediction following myocardial infarction. *Eur Heart J Cardiovasc Imaging* 20:77
9. Gjesdal O, Almeida AL, Hopp E et al (2014) Long axis strain by MRI and echocardiography in a postmyocardial infarct population. *J Magn Reson Imaging* 40:1247–1251
10. Aurich M, Fuchs P, Müller-Hennessen M et al (2018) Unidimensional longitudinal strain: a simple approach for the assessment of longitudinal myocardial deformation by echocardiography. *J Am Soc Echocardiogr* 31:733–742
11. Hung CL, Verma A, Uno H et al (2010) Longitudinal and circumferential strain rate, left ventricular remodeling, and prognosis after myocardial infarction. *J Am Coll Cardiol* 56:1812–1822
12. Ponikowski P, Voors AA, Anker SD et al (2016) 2016 ESC Guidelines for the diagnosis and treatment of acute and chronic heart failure: The Task Force for the diagnosis and treatment of acute and chronic heart failure of the European Society of Cardiology (ESC) developed with the special contribution of the Heart Failure Association (HFA) of the ES. *Eur Heart J* 37:2129–2200
13. Leng S, Tan RS, Zhao XD, Allen JC, Koh AS, Zhong L (2018) Validation of a rapid semi-automated method to assess left atrial longitudinal phasic strains on cine cardiovascular magnetic resonance imaging. *J Cardiovasc Magn Reson* 20:71
14. Leng S, Zhang S, Jiang M et al (2018) Imaging 4D morphology and dynamics of mitral annulus in humans using cardiac cine MR feature tracking. *Sci Rep* 8:81
15. Gonzalez RC, Woods RE (2018) Digital image processing, 4th edn. Pearson/Prentice Hall, New York
16. Leng S, Dong Y, Wu Y et al (2019) Impaired cardiovascular magnetic resonance-derived rapid semiautomated right atrial longitudinal strain is associated with decompensated hemodynamics in pulmonary arterial hypertension. *Circ Cardiovasc Imaging* 12:e008582
17. Leng S, Jiang M, Zhao XD et al (2016) Three-dimensional tricuspid annular motion analysis from cardiac magnetic resonance feature-tracking. *Ann Biomed Eng* 44:3522–3538
18. Leng S, Zhao XD, Huang FQ et al (2015) Automated quantitative assessment of cardiovascular magnetic resonance-derived atrioventricular junction velocities. *Am J Physiol Heart Circ Physiol* 309:H1923–H1935
19. Young AA, Li B, Kirton RS, Cowan BR (2012) Generalized spatiotemporal myocardial strain analysis for DENSE and SPAMM imaging. *Magn Reson Med* 67:1590–1599
20. Dahl JS, Barros-Gomes S, Videbæk L et al (2016) Early diastolic strain rate in relation to systolic and diastolic function and prognosis in aortic stenosis. *JACC Cardiovasc Imaging* 9:519–528
21. Ersbøll M, Andersen MJ, Valeur N et al (2014) Early diastolic strain rate in relation to systolic and diastolic function and prognosis in acute myocardial infarction: a two-dimensional speckle-tracking study. *Eur Heart J* 35:648–656
22. Morris DA, Boldt LH, Eichstädt H, Ozcelik C, Haverkamp W (2012) Myocardial systolic and diastolic performance derived by 2-dimensional speckle tracking echocardiography in heart failure with normal left ventricular ejection fraction. *Circ Heart Fail* 5:610–620
23. Smith SP, Secomb TW, Hong BD, Moulton MJ (2016) Time-dependent regional myocardial strains in patients with heart failure with a preserved ejection fraction. *Biomed Res Int* 2016:8957307
24. Phan TT, Shivu GN, Abozguia K, Gnanadevan M, Ahmed I, Frenneaux M (2009) Left ventricular torsion and strain patterns in heart failure with normal ejection fraction are similar to age-related changes. *Eur J Echocardiogr* 10:793–800
25. Yip G, Wang M, Zhang Y, Fung JW, Ho PY, Sanderson JE (2002) Left ventricular long axis function in diastolic heart failure is reduced in both diastole and systole: time for a redefinition? *Heart* 87:121–125
26. Park JJ, Park JB, Park JH, Cho GY (2018) Global longitudinal strain to predict mortality in patients with acute heart failure. *J Am Coll Cardiol* 71:1947–1957
27. Yu CM, Lin H, Yang H, Kong SL, Zhang Q, Lee SW (2002) Progression of systolic abnormalities in patients with “isolated” diastolic heart failure and diastolic dysfunction. *Circulation* 105:1195–1201
28. Borlaug BA, Redfield MM, Melenovsky V et al (2013) Longitudinal changes in left ventricular stiffness: a community-based study. *Circ Heart Fail* 6:944–952
29. Pascual-Figal DA, Ferrero-Gregori A, Gomez-Otero I et al (2017) Mid-range left ventricular ejection fraction: clinical profile and cause of death in ambulatory patients with chronic heart failure. *Int J Cardiol* 240:265–270
30. Koh AS, Tay WT, Teng THK et al (2017) A comprehensive population-based characterization of heart failure with mid-range ejection fraction. *Eur J Heart Fail* 19:1624–1634
31. Carluccio E, Biagioli P, Mengoni A et al (2018) Left atrial reservoir function and outcome in heart failure with reduced ejection fraction. *Circ Cardiovasc Imaging* 11:e007696
32. Solomon SD, Biering-Sørensen T (2017) LA strain when ejection fraction is preserved: a new measure of diastolic function? *JACC Cardiovasc Imaging* 10:744–746
33. Peng JP, Zhao XD, Zhao L et al (2018) Normal values of myocardial deformation assessed by cardiovascular magnetic resonance feature tracking in a healthy Chinese population: a multicenter study. *Front Physiol* 9:1181
34. Shang Q, Patel S, Steinmetz M et al (2018) Myocardial deformation assessed by longitudinal strain: chamber specific normative data for CMR-feature tracking from the German competence network for congenital heart defects. *Eur Radiol* 28:1257–1266
35. Voigt JU, Pedrizzetti G, Lysyansky P et al (2015) Definitions for a common standard for 2D speckle tracking echocardiography: consensus document of the EACVI/ASE/industry task force to standardize deformation imaging. *J Am Soc Echocardiogr* 28:183–193
36. Amzulescu MS, De Craene M, Langet H et al (2019) Myocardial strain imaging: review of general principles, validation, and sources of discrepancies. *Eur Heart J Cardiovasc Imaging* 20:605–619
37. Kempny A, Fernández-Jiménez R, Orwat S et al (2012) Quantification of biventricular myocardial function using cardiac magnetic resonance feature tracking, endocardial border delineation and echocardiographic speckle tracking in patients with repaired tetralogy of Fallot and healthy controls. *J Cardiovasc Magn Reson* 14:32
38. Lamacie MM, Houbois CP, Greiser A, Jolly MP, Thavendiranathan P, Wintersperger BJ (2019) Quantification of myocardial deformation by deformable registration-based analysis of cine MRI: validation with tagged CMR. *Eur Radiol* 29:3658–3668